water

MDPI

Article

Effect of Deficit Irrigation on Nitrogen Uptake of Sunflower in the Low Desert Region of California

Mohamed Galal Eltarabily [1,2,*], John M. Burke [3] and Khaled M. Bali [1]

1 Kearney Agricultural Research and Extension Center, University of California, Parlier, CA 93648, USA; kmbali@ucanr.edu
2 Civil Engineering Department, Faculty of Engineering, Port Said University, Port Said 42523, Egypt
3 Department of Plant Biology, University of Georgia, Miller Plant Sciences, Athens, GA 30602, USA; jmburke@uga.edu
* Correspondence: meltarabily@ucdavis.edu or eng_m_trabily@eng.psu.edu.eg

Received: 8 October 2019; Accepted: 5 November 2019; Published: 8 November 2019

Abstract: Nitrogen (N) accounts for more than 80% of the total mineral nutrients absorbed by plants and it is the most widely limiting element for crop production, particularly under water deficit conditions. For a comprehensive understanding of sunflower *Helianthus annuus* N uptake under deficit irrigation conditions, experimental and numerical simulation studies were conducted for full (100% ET_C) and deficit (65% ET_C) irrigation practices under the semi-arid conditions of the Imperial Valley, California, USA. Plants were established with overhead sprinkler irrigation before transitioning to subsurface drip irrigation (SDI). Based on pre-plant soil N testing, 39 kg ha^{-1} of N and 78 kg ha^{-1} of P were applied as a pre-plant dry fertilizer in the form of monoammonium phosphate (MAP) and an additional application of 33 kg ha^{-1} of N from urea ammonium nitrate (UAN-32) liquid fertilizer was made during the growing season. Soil samples at 15-cm depth increments to 1.2 m (8 layers, 15 cm each) were collected prior to planting and at three additional time points from two locations each in the full and deficit irrigation treatments. We used HYDRUS/2D for the simulation in this study and the model was calibrated for the soil moisture parameters (θ_s and θ_r), the rate constant factors of nitrification (the sensitive parameter) in the liquid and solid states ($\mu_{w,3}$, and $\mu_{s,3}$). The HYDRUS model predicted cumulative root water uptake fluxes of 533 mm and 337 mm for the 100% ET_C and 65% ET_C, respectively. The simulated cumulative drainage depths were 23.7 mm and 20.4 mm for the 100% ET_C and 65% ET_C which represented only 4% and 5% of the applied irrigation water, respectively. The soil wetting profile after SDI irrigation was mostly around emitters for the last four SDI irrigation events, while the maximum values of soil moisture in the top 30 cm of the soil profile were 0.262 cm^3 cm^{-3} and 0.129 cm^3 cm^{-3} for 100% ET_C and 65% ET_C, respectively. The 16.5 kg ha^{-1} $(NH_2)_2CO$ (50% of the total N) that was applied during the growing season was completely hydrolyzed to NH_4^+ within 7 days of application, while 4.36 mg cm^{-1} cumulative decay was achieved by the end of the 98-day growing season. We found that 86% of NH_4^+ (74.25 mg cm^{-1}) was nitrified to NO_3^- while 14% remained in the top 50 cm of the soil profile. The denitrification and free drainage of NO_3^- were similar for 100% ET_C and 65% ET_C, and the maximum nitrate was drained during the sprinkler irrigation period. By the end of the growing season, 30.8 mg cm^{-1} of nitrate was denitrified to N_2 and the reduction of nitrate plant uptake was 17.1% for the deficit irrigation section as compared to the fully irrigated side (19.44 mg cm^{-1} vs. 16.12 mg cm^{-1}). This reduction in N uptake due to deficit irrigation on sunflower could help farmers conserve resources by reducing the amount of fertilizer required if deficit irrigation practices are implemented due to the limited availability of irrigation water.

Keywords: deficit irrigation; monoammonium phosphate (MAP); urea ammonium nitrate (UAN-32); nitrification; HYDRUS/2D; Imperial Valley; California

1. Introduction

Nitrogen (N) plays a vital role in plants as a major component of chlorophyll (i.e., photosynthesis) and amino acids (the building blocks of protein) [1]. Phosphorus (P) is essential for respiration, energy storage and transfer, and cell division and enlargement [2]. Understanding N and P cycles within the soil-plant system in response to water stress is becoming crucial [3]. Drought stress or water deficit in the root zone affect plant vigor and survivorship by reducing N and P uptake, transport, and distribution processes [4,5]. This reduction is directly correlated with the decline in soil moisture [6] and accompanies a reduction of photosynthesis and transpiration [7]. When deficit irrigation practices are implemented, nutrient diffusion and mass flow in the soil decrease [8] and nutrient supply through mineralization is negatively affected [9]. Deficit irrigation during a specific stage of growth (followed by no irrigation or fully drying) negatively affects nutrient uptake [10], whereas a regulated deficit (i.e., with drying–rewetting cycles) enhances mineralization [11]. During drought stress or deficit irrigation, the N and P cycles are altered [12] where the diffusivity of P in soil is more sensitive to soil moisture than that of N [9].

Sunflower (*Helianthus annuus*) is a major oilseed crop that is often grown in arid or semi-arid regions. The nutrient input requirements of sunflower depend on soil fertility [13,14] and irrigation water quality [15], and a comprehensive understanding of drought stress during water deficit conditions is needed to achieve the target yield. Pre-plant soil tests are needed to define the residual nitrate and phosphate levels in soil [16,17] and can be used as the basis to determine the required amounts of P and N during the growing season [18]. About 15 kg N ha^{-1} from monoammonium phosphate (MAP), 11-52-0, is recommended as starter dry fertilizer at planting, or 25 kg N ha^{-1} from urea ammonium nitrate (UAN-32) liquid fertilizer can be injected into drip lines [19]. In California, urea or diammonium phosphate (either 18-46-0 or 16-48-0) are not recommended [20] due to potential degradation of soil properties [21]. In addition to dry MAP application [20], 100 kg P_2O_5 h^{-1} (~45 kg P ha^{-1}) is sufficient [22]. Due to the inherent complexity of the N cycle and the difficulty in directly measuring the various fluxes of N [23], obtaining a complete N mass balance is extremely challenging [24]. Numerous studies of N budget analysis in agricultural fields [25–30] concluded that the nitrate leaching could be substantial and depends mainly on the rate of applied fertilizer, source of N, soil types, and the amount of rainfall water.

Nitrogen is present in the soil in nine different forms, including intermediaries of subsequent transformations, corresponding to different oxidative states [31,32]. HYDRUS software (developed by [33]) is widely used as a finite element model for simulating the movement of water, N transport, and the transformation process in variably saturated soil [34–37]. The governing convection–dispersion solute transport equations are written in a relatively general form by including provisions for non-linear, non-equilibrium reactions between the solid and liquid phases and linear equilibrium reactions between the liquid and gaseous phases [36]. The solute transport equations further incorporate the effects of zero-order production, first-order degradation independent of other solutes, and first-order decay for various N species. Deficit irrigation practices generally reduce crop yield and may have adverse effects on nutrient uptake and net assimilation, and can thus directly impact nitrogen uptake [38]. Insufficient soil moisture can also negatively impact nutrient use efficiency (NUE) through its direct impact on mechanisms such as volatilization and denitrification [39]. As a result, crops generally suffer from nutrient deficiencies under water stress and become more sensitive to N_2 fixation under drying soil conditions and high-temperature stress associated with arid conditions or deficit irrigation [40].

While the final leaching of N below the root zone is in the form of nitrate [41], few studies have discussed all potential mechanisms of N transformation associated with water deficit under arid conditions. Therefore, the objective of this study was to identify the effect of water stress due to the implementation of a 65% crop evapotranspiration (ET_C) deficit irrigation regime on nitrate root uptake and the transport and transformation N processes in the root zone of sunflower planted in the semi-arid region of the Imperial Valley, California. This irrigation regime represents a baseline that provides ca. one-third savings in applied water while still providing generally acceptable yields.

The main source of N in this study was from fertilizer applications in the form of MAP and UAN-32. The transformation processes of interest were: mineralization and fixation, volatilization, hydrolysis, nitrification, and denitrification. HYDRUS/2D was utilized to simulate the water and nitrate uptake after calibration of moisture content and saturated hydraulic conductivity, as well as the first-order decay parameter of nitrate denitrification in the liquid and solid phases.

2. Material and Methods

2.1. Study Area and Sunflower Water Use

The experiment was carried out on a 4520 m^2 (0.45 ha; 73.5 m long × 61.5 m wide) research plot located at 32°48′24″ N, 115°26′43″ W at the University of California Desert Research and Extension Center (DREC) in Imperial Valley, near Holtville, CA, USA (Figure 1a). The soil type is classified as Glenbar silty clay loam [42], and the region is classified as a semi-arid area with an annual rainfall amount of less than 75 mm/year. Seeds were planted on 26 March 2019 and harvested after 98 days on 1 July, based on a growing degree day (GDD) model (1982C to full maturity on 15 June and 2460C to completion of grain filling). We used reference evapotranspiration (ET_O) from a nearby California Irrigation Management Information System (CIMIS) located at DREC (CIMIS weather station number 87) [43]. We used crop coefficients (K_{CS}) of 0.2, 1.1, and 0.4 for the initial stage (20 days), mid-stage (43 days), and late-season (15 days), respectively, and 29 days for the developing stage during which the values ranged from 0.2 to 1.1 [44]. Weekly sunflower crop evapotranspiration (ET_C) amounts were estimated from ET_O and K_C and used to calculate the required irrigation applications (Table 1).

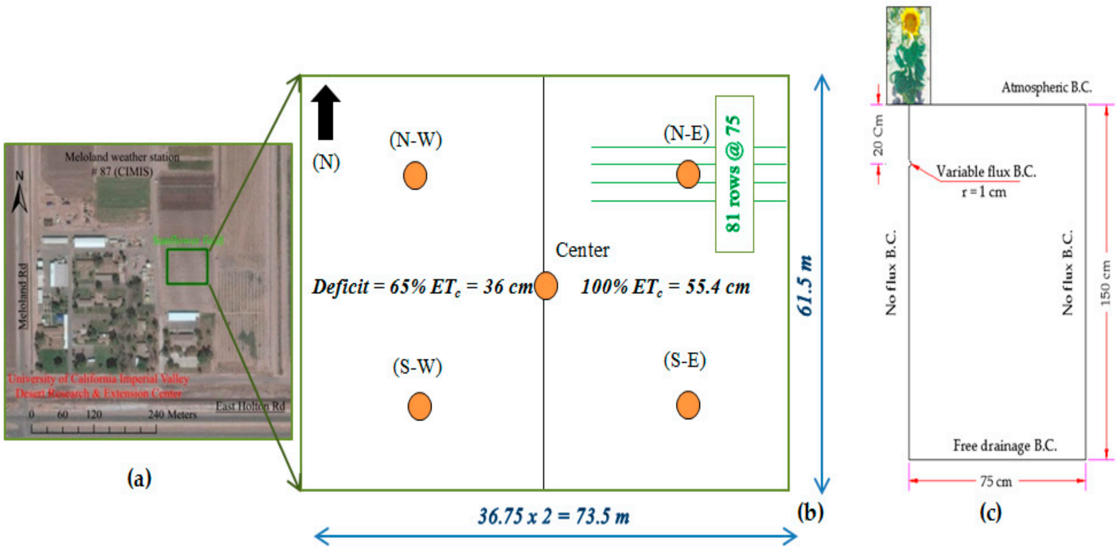

Figure 1. (**a**) Location of the sunflower plot at University of California Desert Research and Extension Center (DREC); (**b**) layout plan of the field showing the deficit and full irrigation sections and the five locations of groundwater observation wells and soil samples; and (**c**) simulation model domain showing the boundary conditions. B.C.: boundary condition.

Table 1. Evapotranspiration reference (California Irrigation Management Information System, CIMIS) and crop coefficient for each growing stage including irrigation water (mm-ha/ha) from sprinkler and subsurface drip irrigation (SDI), and dates of fertilizer application. MAP: monoammonium phosphate fertilizer; UAN-32: urea ammonium nitrate liquid fertilizer.

Stage	Days	Period	K_C	ET_o (cm)	ET_C (cm)	Irrigation (mm-ha/ha)	Fertilizers
Initial	20	26 March–14 April	0.2	12.76	2.55	Sprinkler 27/3—19/4 (175) SDI 19/4—1/7 65% ETc (185) 100% ETc (379)	350 kg ha^{-1} MAP on 26 March prior to the first sprinkler application of 275 m^3 103 kg ha^{-1} UAN-32 on 16 May with 353 m^3 of 4 SDI event
Crop development	29	15 April–13 May	0.2–1.1	21.25	14.07		
Mid-season	34	14 May–16 June	1.1	27.22	29.94		
Late season	16	17 June–1 July	1.1–0.4	12.31	8.81		
Total	98	26 March–1 July	K_C avg. = 0.75	73.54	**55.37**		

2.2. Planting, Irrigation, and Fertigation Scheduling

Prior to planting, we installed a subsurface drip irrigation (SDI) system at a depth of 30 cm below the soil surface. Sunflower seeds of the grey stripe mammoth variety (Mountain Valley Seed Co., Salt Lake City, Utah, USA) were plated in 75-cm row spacing oriented from east to west, and hand-moved sprinkler irrigation was used for germination and applied from 26 March to 19 April (0.25 cm h^{-1} application rate using a Nelson R2000WF rotator sprinkler system). Eleven sprinkler events were applied during that period and a total of 175 mm-ha/ha were used for germination and stand establishment. We then utilized the previously installed SDI system (application rate of 0.18 cm h^{-1} with 30-cm emitter spacing, 2-cm drip tape diameter, and drip line spacing of 75 cm or one drip line per row of sunflower) for irrigation through the end of the growing season. The field was divided into two irrigation treatments where the west section received only 65% (deficit irrigation) of the expected ET_C and the east side received 100% (full irrigation) of the expected ET_C. The 65% ET_C deficit treatment was selected to represent ca. one-third savings in applied water, which would generate approximately 194 mm-ha/ha of water savings and could help growers meet the conservation goals for water transfer from the Imperial Valley to San Diego [45]. In addition, previous sunflower work conducted at DREC resulted in marginal yield reductions that could be offset by the value of the water savings at deficit irrigation levels near 60% ET_C.

Irrigation events were scheduled weekly using the estimated ET_C, and nine total SDI irrigation events were applied. The full irrigation treatment received an additional 379 mm-ha/ha, while the deficit half of the field received only an additional 185 mm-ha/ha to achieve the season-long deficit irrigation corresponding to 65% ET_C; this was reached on 7 June after the 5 SDI event. Pre-plant soil chemical analysis and groundwater hydrochemical tests were performed to determine the required amount of fertilizers based on our target yield. Soil samples were collected from five locations at eight 15-cm depth increments representing the entire root zone of 1.2 m (effective root depth) [46]. Five groundwater observation wells were installed close to the soil sampling locations, and water table depth and groundwater samples were collected weekly (Figure 1b). We applied 350 kg ha^{-1} MAP 11-52-0 as a pre-plant dry fertilizer on 26 March, and an additional 103 kg ha^{-1} of UAN-32 was subsequently applied as a nitrogen supplement for the entire field via the SDI system on 16 May (during the flowering stage). Two sets of tests for salinity, chloride, pH, nitrate, phosphate, and organic matter were performed on the samples collected from the five soil sampling locations on 9 April (after MAP application) and 28 June (just before harvest). These samples were sent to an outside lab for analysis (Ward Laboratories, Inc., Kearney, NE; Supplementary Table S1).

2.3. Transformation Processes and Mass Balance

The starter application of 39 kg ha^{-1} of N was applied on 26 March and was followed by a 61 mm-ha/ha sprinkler event (first sprinkler event, 24 h) with the expected nitrification to nitrite, NO_2^-, followed by oxidation to nitrate, NO_3^-. The 33 kg ha^{-1} of N from the 103 kg ha^{-1} of UAN-32 that was applied on 16 May with 78 mm-ha/ha irrigation water (fourth SDI event) corresponded to 8.25 kg ha^{-1}

NO_3^- (nitrate), which was available for plant uptake as soon as it reached the root zone, 8.25 kg ha^{-1} NH_4^+ (ammonium), and 16.5 kg ha^{-1} $(NH_2)_2CO$-N (urea) that moved freely with soil-water until hydrolyzed by urease enzyme to form ammonic nitrogen that held to the clay soil particles before being converted to nitrate by soil organisms within a few weeks. Thus, the third-type Cauchy boundary condition (B.C.) was set at the top edge of the simulation domain and along the periphery of the emitter. The partial differential equations governing the advection-dispersion of urea, ammonium, and nitrate in two dimensions are determined by [37] from the one-dimension equations by [33] as follows:

Urea, $(NH_2)_2CO$–N:

$$\begin{aligned}\frac{\partial\theta\,(c_{w,1})}{\partial t} = \frac{\partial}{\partial x}\left(\theta D_{1\ x,x}\frac{\partial c_{w,1}}{\partial x} + \theta D_{1\ x,z}\frac{\partial c_{w,1}}{\partial z}\right) + \frac{\partial}{\partial z}\left(\theta D_{1\ z,z}\frac{\partial c_{w,1}}{\partial z} + \theta D_{1\ z,x}\frac{\partial c_{w,1}}{\partial x}\right) \\ -\left(\frac{\partial q_x\,(c_{w,1})}{\partial x} + \frac{\partial q_z\,(c_{w,1})}{\partial z}\right) - \mu'_{w,1}\theta(c_{w,1}),\end{aligned} \tag{1}$$

Ammonium, NH_4^+–N:

$$\begin{aligned}\frac{\partial\theta\,(c_{w,2})}{\partial t} + \rho\,\frac{\partial c_{s,2}}{\partial t} = \frac{\partial}{\partial x}\left(\theta D_{2\ x,x}\frac{\partial c_{w,2}}{\partial x} + \theta D_{2\ x,z}\frac{\partial c_{w,2}}{\partial z}\right) + \frac{\partial}{\partial z}\left(\theta D_{2\ z,z}\frac{\partial c_{w,2}}{\partial z} + \theta D_{2\ z,x}\frac{\partial c_{w,2}}{\partial x}\right) \\ -\left(\frac{\partial q_x(c_{w,2})}{\partial x} + \frac{\partial q_z(c_{w,2})}{\partial z}\right) + \mu'_{w,1}\theta(c_{w,1}) - (\mu_{w,2} + \mu'_{w,2})\,\theta(c_{w,2}) - (\mu_{s,2} + \mu'_{s,2})\,\rho(c_{s,2}) + \gamma_{w,2}\theta + \\ \gamma_{s,2}\rho - S(X,Z,\,T)(c_{w,2}),\end{aligned} \tag{2}$$

Nitrate, NO_3^-–N:

$$\begin{aligned}\frac{\partial\theta\,(c_{w,3})}{\partial t} = \frac{\partial}{\partial x}\left(\theta D_{3\ x,x}\frac{\partial c_{w,3}}{\partial x} + \theta D_{3\ x,z}\frac{\partial c_{w,3}}{\partial z}\right) + \frac{\partial}{\partial z}\left(\theta D_{3\ z,z}\frac{\partial c_{w,3}}{\partial z} + \theta D_{3\ z,x}\frac{\partial c_{w,3}}{\partial x}\right) - \left(\frac{\partial q_x(c_{w,3})}{\partial x} + \frac{\partial q_z(c_{w,3})}{\partial z}\right) \\ + \mu'_{w,2}\,\theta(c_{w,2}) + \mu'_{s,2}\,\rho(c_{s,2}) - (\mu_{w,3} + \mu_{s,3})\,\theta(c_{w,3}) - S(X,Z,\,T)(c_{w,3}),\end{aligned} \tag{3}$$

where subscripts 1, 2, and 3 represent $(NH_2)_2CO$, NH_4^-, and NO_3^-, respectively, while w and s are the liquid and solid phases of nitrogen. C is the concentration in the soil solution (g cm^{-3}) and ρ is the soil dry bulk density (g cm^{-3}). $D_{x,x}$, $D_{z,z}$, and $D_{x,z}$ are the components of the dispersion tensor (cm^2 day^{-1}) while the dispersion coefficient in the liquid phase, D, is given by $\theta D = D_L|q| + \theta D_w^0\,\tau_w$, where D_w^0 is the molecular diffusion coefficient in free water (cm^2 day^{-1}), τ_w is the tortuosity factor in the liquid phase, and D_L is the longitudinal dispersivity (cm). q_x and q_z are the volumetric water flux components (cm day^{-1}) and μ represents the first-order transformation rate constant of N (d^{-1}). μ' is the first-order rate constant between urea and nitrate. γ is the zero-order transformation rate constant of N (g cm^{-3} day^{-1}) and $S(X, Z, T)$ is the passive root nutrient uptake. The initial assignment of these parameters was based on previous studies [47–49] in addition to the soil properties; the Vrugt model and Feddes' parameters are shown in Table 2. The water stress response function that was suggested by Feddes [50] was used in the simulation to estimate the impact of water stress on the potential root water uptake. The above function was used since the crop coefficients found in the literature typically report crop coefficients based on unstressed conditions. When the deficit irrigation was implemented during this study, soil moisture content and actual crop evapotranspiration reached stress stage [51] which resulted in crop coefficients lower than what is expected under unstressed conditions.

Table 2. Soil physical parameters, transport and transformation parameters, and root distribution and uptake parameters.

Basic Physical Soil Properties of the Experimental Field [42]									
USDA [a] Texture	**Soil Layer**	**Composition Sand, Silt, Clay**	**ρ_b (g cm^{-3})**	**θ_f (cm^3 cm^{-3})**	**Parameters of the Water Retention Equation (Van Genuchten Model)**				
					θ_r (cm^3 cm^{-3})	**θ_s (cm^3 cm^{-3})**	**α (cm^{-1})**	**n**	**K_s (cm day^{-1})**
Silty clay loam [1]	0.0–0.30 m	17%, 48%, 35%	1.50	0.325	0.084	**0.424** * (0.41–0.44)	0.009	1.451	**5.28** * (4.0–7.0)
Silty clay [2] and clay	0.30–1.50 m	18%, 42%, 40%	1.45	0.351	0.089	**0.445** * (0.41–0.44)	0.012	1.403	**6.99** * (4.0–7.0)

Initial and Calibrated N Transport and Transformation Parameters for the Model Simulation										
	D_L (cm)	$\mu'_{w,1}$(day^{-1})	$\mu_{w,2}$(day^{-1})	$\mu'_{w,2}$ (day^{-1})	$\mu'_{s,2}$ (day^{-1})	$\mu_{w,3}$ (day^{-1})	$\mu_{s,3}$ (day^{-1})	$\gamma_{w,2}$ (day^{-1})	$\gamma_{s,2}$ (day^{-1})	K_d
	5.0	(0.3–0.8)	(0.02–0.07)	(0.02–0.72)	(0.02–0.72)	(0.01–0.24)	(0.01–0.24)	(0.001–0.04)	(0.001–0.04)	3–4
Soil 1	5.0	0.45	0.02	0.20	0.20	**0.020** *	**0.020** *	0.001	0.001	3.50
Soil 2	5.0	0.45	0.02	0.20	0.20	**0.010** *	**0.010** *	0.001	0.001	3.50

Vrugt Model for Sunflower Root Distribution Parameters [52]					
z_{1m} (cm)	z_1 (cm)	P_z	x_{1m} (cm)	x_1 (cm)	P_x
150	120	1	75	30	1

Feddes' Parameters (Root Water Uptake Parameters for Sunflower) [50]						
P_0 (cm)	P_{opt} (cm)	P2H (cm)	P2L (cm)	P3 (cm)	r2H (cm day^{-1})	r2L (cm day^{-1})
−1	−5	−400	−500	−10,000	0.5	0.1

Note: [a] United States Department of Agriculture, National Resources Conservation Service, (bold *) is the calibrated parameter. ρ_b, bulk density; θ_f, field capacity; θ_r, residual volumetric water contents; θ_s, saturated volumetric water contents; α and n, fitting parameters of the soil–water characteristic curve; K_s, saturated hydraulic conductivity. Mineralization and fixation by the zero-order decay chain as $\gamma_{w,2}\theta$ and $\gamma_{s,2}\theta$. Volatilization was expressed by the first-order rate as $\mu_2\ \theta c_2$. Nitrification of NH_4^+–N to NO_3^-–N was expressed by the first-order reactions $\mu'_{w,2}\ \theta(c_{w,2})$ and $\mu'_{s,2}\ \rho(c_{s,2})$ for the N in the liquid and solid phase, respectively. Denitrification was expressed by the first-order decay chains as $(\mu_{w,3})\ \theta(c_{w,3})$ and $(\mu_{s,3})\ \rho(c_{s,3})$. Adsorption of NH_4^+–N by soil linear adsorption isotherm, where K_d is the distribution coefficient of NH_4^+–N between liquid and solid phases. $\mu'_{w,1}$, the first-order rate constant of hydrolysis; $\mu_{w,2}$, the first-order decay coefficient of volatilization; $\mu'_{w,2}$ and $\mu'_{s,2}$, respectively the first-order rate constants of nitrification in the liquid and solid phases; $\mu_{w,3}$ and $\mu_{s,3}$, respectively the first-order decay rate constants of denitrification; $\gamma_{w,2}$ and $\gamma_{s,2}$, the mineralization zero-order decay in liquid and solid states; P_0, value of the pressure head below which roots start to extract water from the soil; P_{opt}, value of the pressure head below which roots extract water at the maximum possible rate; P2H, value of the limiting pressure head below which roots can no longer extract water at the maximum rate; P2L, as P2H, but for a potential transpiration rate of r2L; P3, value of the pressure head below which root water uptake ceases (usually taken at the wilting point).

The boundary conditions of the simulated domain are shown in Figure 1c as no flux along the vertical sides of the domain because of the symmetry and the extent of the area at the left and right sides, respectively. While the water table was at 1.80 m (below the bottom edge of the model domain (1.50 m)), the bottom edge was assigned as a free drainage boundary condition (B.C.) and the ground surface was assigned as a variable flux during sprinkler irrigation events and atmospheric flux was set to represent the evapotranspiration ET_C along the 75 cm width (sunflower row spacing). The variable flux for sprinkler (Val.1) and drip tape (Val.2) was set to swiftly change between constant flux during irrigation and zero (no flux) after the termination of irrigation events. We assigned 117 time-variable boundary conditions to include the daily time step between the 98-day growing season and times of irrigation; the corresponding ET_C values between irrigation events were calculated from the hourly ET_o records of the nearby CIMIS weather station #87 (approximately 300 m from the experimental site) and assigned for each interval. The two defined soil layers representing the full and deficit irrigation treatments were assigned, and four observation nodes along the 120 cm depth at 30 cm increments were pointed below the drip lines (the left edge) to express the locations of the collected soil samples. The model was first run for water flow and root-water uptake, then soil moisture content and hydraulic conductivity were calibrated based on the soil moisture measurements using Irrometer Watermark readings at specified times for both the deficit and full irrigation treatments. Thereafter, the solute transport process was executed to simulate the transport and transformation of N, and the NO_3–N concentrations were calibrated with the N concentrations in the collected soil samples on 9 April and 28 June where the initial nitrate concentration was 0.02 mg cm^{-3}. Finally, the root nutrient uptake was computed, and the nitrogen mass balance was performed for the full (100% ET_C) and deficit (65% ET_C) irrigation treatments.

3. Results

3.1. Root Water Uptake and Model Calibration

The research field at DREC was two-dimensionally simulated using HYDRUS/2D. The model first simulated root water uptake after the initial assignment of soil properties and root distribution parameters, and then the volumetric water content was calibrated with the values obtained from the collected soil samples. In order to validate the model results for root water uptake, the calibration of saturated moisture content, θ_s, and saturated hydraulic conductivity, K_s, was carried out. The soil samples were collected from five locations at the beginning, middle, and end of the growing season, on 9 April, 9 May, and 28 June at eight 15 cm depth increments to the 120 cm. The values of the measured average moisture contents of the four locations and the simulation from HYDRUS are shown in Table 3. The r^2 of observed and simulated moisture content was 0.922 (Figure 2); values of θ_s = 0.424 cm^3 cm^{-3} and 0.445 cm^3 cm^{-3} and K_s = 5.28 cm day^{-1} and 6.99 cm day^{-1} were obtained for silty clay loam and silty clay soil, respectively. As expected, the maximum values of measured and simulated volumetric moisture contents were obtained just after the sixth sprinkler event on 8 April. Both the measured and simulated values on that date were similar for depths at or below 105 cm, which is below the active root zone. The model overestimated the soil moisture contents at depths between 15 and 90 cm (in the active root zone). The model uses ET_o and crop coefficient values to estimate soil moisture content; the estimated soil moisture contents could be overestimated because the model does not account for higher K_C due to the frequent wetting events associated with sprinkler irrigation. The measured soil moisture content on 9 April reflects the actual conditions and suggests that the ET_C during the sprinkler irrigation period was higher than calculated, which resulted in more soil moisture depletion and lower soil moisture content. As expected, both the measured and simulated soil moisture increased with depth, likely due to active uptake by plant roots where most of the uptake is in the top 75 cm of the soil profile. Moisture evaporation from shallower soils could also have contributed to the observed pattern. Both the measured and estimated soil moisture content during the drip irrigation events on and after 9 May were very similar (Table 3).

Table 3. Volumetric water content, θ (cm^3 cm^{-3}), for the soil samples collected on 9 April, 9 May, and 28 June, and the corresponding HYDRUS values.

Depth (cm)	9 April		9 May		28 June			
					100% ET_C		65% ET_C	
	Soil Samples	HYDRUS	Soil Samples	HYDRUS	Soil Samples	HYDRUS	Soil Samples	HYDRUS
15.0	0.305	0.396	0.281	0.293	0.363	0.352	0.130	0.129
30.0	0.328	0.417	0.317	0.305	0.343	0.354	0.133	0.141
45.0	0.378	0.420	0.317	0.309	0.358	0.335	0.145	0.141
60.0	0.386	0.425	0.301	0.317	0.300	0.226	0.142	0.141
75.0	0.370	0.428	0.301	0.325	0.191	0.141	0.162	0.141
90.0	0.403	0.430	0.340	0.333	0.121	0.141	0.135	0.141
105.0	0.424	0.432	0.353	0.342	0.152	0.141	0.148	0.141
120.0	0.423	0.433	0.361	0.349	0.154	0.161	0.171	0.161
150.0	0.442	0.435	-	-	-	-	-	-

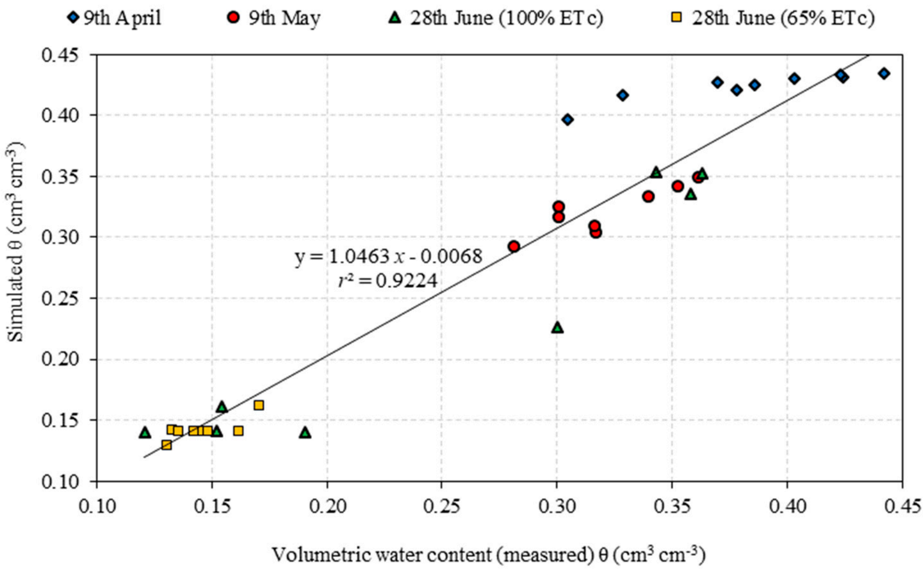

Figure 2. Simulated (HYDRUS) vs. observed (soil samples) moisture content along the 120 cm depth.

The 1.50 m (depth) × 75 cm (width) model domain represented the two sections of 100% ET_C and 65% ET_C while the top 30 cm was silty clay loam and silty clay extended from 30 cm to the bottom edge of the domain (1.50 m). Figure 3 shows the expected sunflower evapotranspiration, the product of multiplying the daily reference ET_O by the K_C used during the simulation. An initial uniform moisture content of 0.244 cm^3 cm^{-3} was used, and the first sprinkler irrigation was applied on 27 March, the day after planting. Just after the end of the first sprinkler irrigation, the moisture content reached the maximum, 0.422 cm^3 cm^{-3}, along the top 20 cm of the soil. Before applying the second sprinkler irrigation on 30 March, the moisture content had declined to 0.325 cm^3 cm^{-3} along the top 20 cm. After germination and stand establishment with sprinkler irrigation, the irrigation system was transitioned to SDI. While the last sprinkler irrigation (eleventh event) was on 19 April, the obtained moisture content just before applying the following SDI irrigation (first drip) on 25 April was nearly uniform for the top 40 cm of soil depth, 0.296 cm^3 cm^{-3}, and gradually declined along the remaining 110 cm from 0.296 cm^3 cm^{-3} to 0.212 cm^3 cm^{-3}. The distribution of the soil moisture content on specific dates throughout the growing seasons is shown in Figure 4.

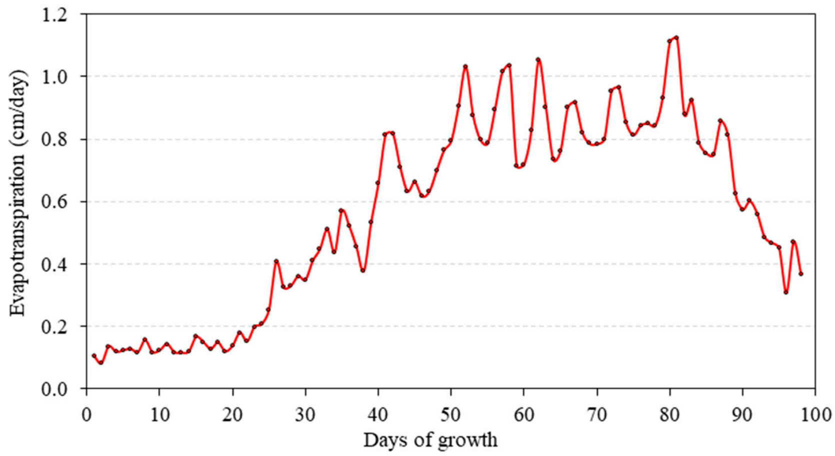

Figure 3. Sunflower evapotranspiration (cm/day) from the daily ET_o (CIMIS weather station #87) and K_C using the values from [44].

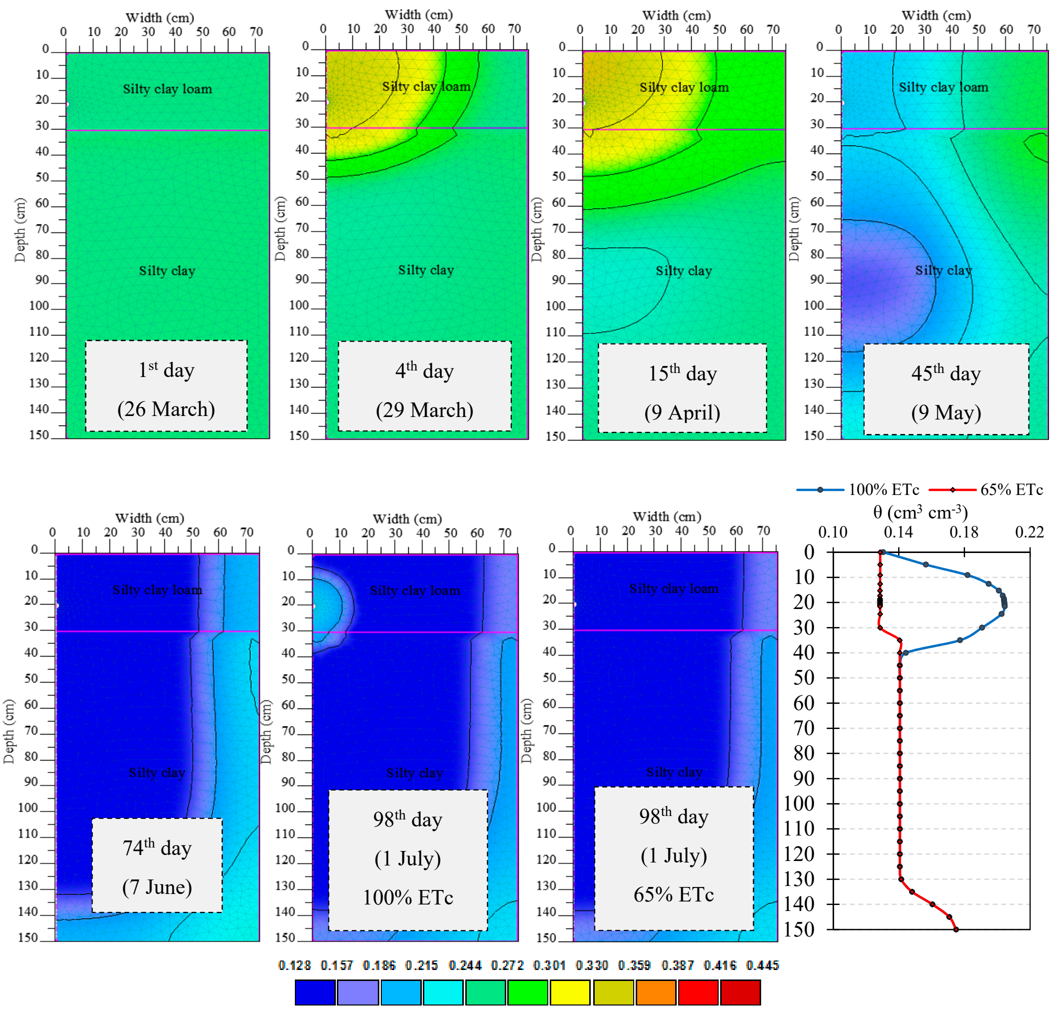

Figure 4. Volumetric moisture content, θ (cm^3 cm^{-3}), during sprinkler irrigation from 26 March to 20 April and SDI from 1 April to 1 July.

It is clear that the distribution of moisture content among the drip events between 25 April and 28 June was different than that from the sprinkler irrigation (Figure 4). During the SDI events, the wetted area was localized around the emitters and the replenishment of moisture content occurred locally around the drip lines. Between 25 April and 10 May, just after the end of the first drip event and just before starting the second drip event, the moisture content at the emitter declined from 0.387 cm^3 cm^{-3} to 0.197 cm^3 cm^{-3}. Just before applying the fourth drip irrigation on 16 May, the moisture content at the emitter was 0.183 cm^3 cm^{-3} and the minimum value, 0.143 cm^3 cm^{-3}, was obtained at 90 cm depth. During the 21 days between the fourth and fifth drip irrigation, which occurred on 7 June, the moisture content was substantially reduced along the 1.50 m soil profile where it was 0.128 cm^3 cm^{-3} for the top 30 cm and 0.141 cm^3 cm^{-3} for the rest of the 120 cm depth. After the fifth drip irrigation on 7 June, the 65% ET_C (36 cm, applied irrigation water) was reached for the western half of the field (deficit irrigation treatment) and no additional irrigation water was applied after that date. By the end of the growing season, 1 July, the moisture content for the deficit half of the field reached a minimum value of 0.128 cm^3 cm^{-3} for almost the entire root zone. For the full irrigated side of the field, four more drip events were applied between 20 June and 28 June to reach 100% ET_C. Just after finishing the sixth drip irrigation, the moisture content was 0.365 cm^3 cm^{-3} around the emitter while the radius of the wetted area was only ca. 30 cm in diameter. After the last drip irrigation on 28 June, the wetted area slightly expanded around the emitter with a diameter of ca. 40 cm and an average moisture content of 0.141 cm^3 cm^{-3} for the entire 120 cm of the domain.

In the model simulation, eleven sprinkler events and nine drip events represented the influx for the model domain for the fully irrigated (100% ET_C) treatment, while eleven sprinkler events and five drip events represent the influx to the model for the deficit (65% ET_C) treatment. No precipitation was assigned to the model because there was no recorded rainfall obtained from the nearby CIMIS weather station. The out-flux was represented by root uptake and the drainage flux by the bottom boundary to the groundwater. The single fluxes are shown in Figure 5a,b for 65% ET_C and 100% ET_C, respectively. It is clear from model simulation and soil moisture measurements that the actual root water uptake was quite different for the 65% ET_C and 100% ET_C treatments after 60 days of growth. The sprinkler flux was assigned for the full width of the top 75 cm and the drip flux was assigned along the perimeter of the emitter. A flux of 6.1 cm day^{-1} was assigned for the sprinkler irrigation where the total applied water was 17.5 cm from 69 total hours of operation. A flux of 9.298 cm day^{-1} was assigned for the drip irrigation where five events give 18.374 cm and the nine events gave 37.748 cm. The cumulative in- and out-fluxes are shown in Figure 5c,d where the total root water uptakes during the season were 532.63 mm and 337.23 mm for the 100% ET_C and 65% ET_C treatments, respectively. Additionally, the cumulative drainages were 23.68 mm and 20.35 mm for the 100% ET_C and 65% ET_C treatments, which represent only 4% and 5% of the applied irrigation water, respectively. That was interpreted as being due to the low infiltration rate of the silty clay loam and silty clay soil that represent the model domain.

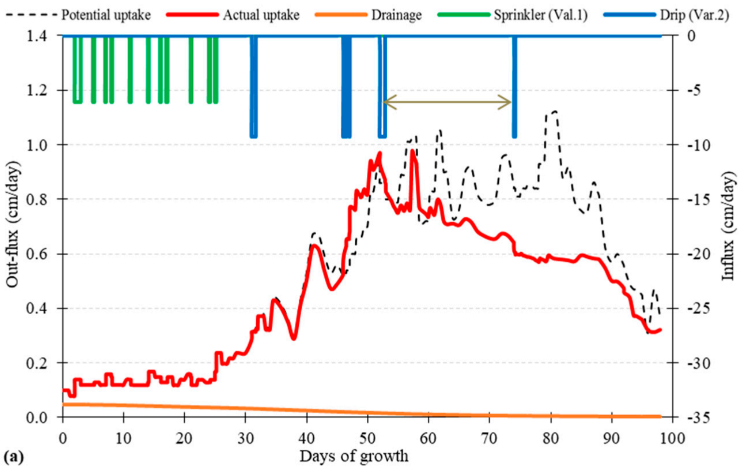

Figure 5. *Cont.*

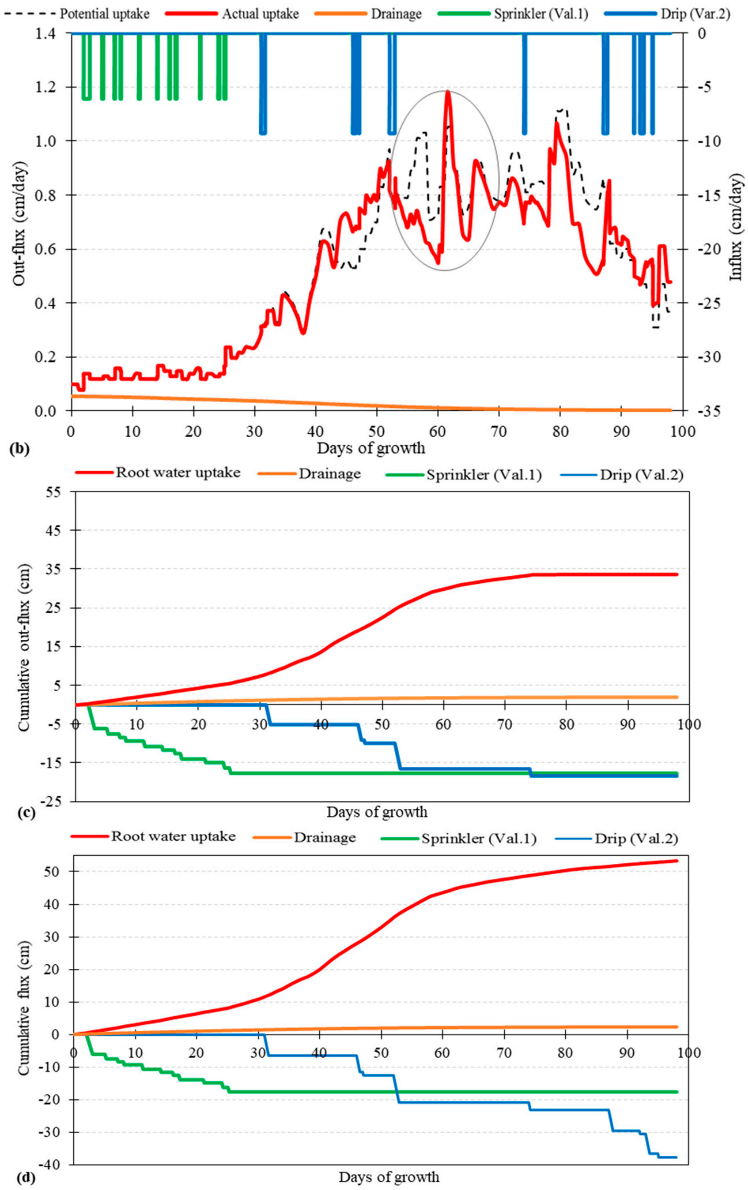

Figure 5. Visualization of in- and out-fluxes. (**a**) Single fluxes (cm day^{-1}) for 65% ET_C. (**b**) Single fluxes (cm day^{-1}) for 100% ET_C. (**c**) Cumulative fluxes (cm) for 65% ET_C. (**d**) Cumulative fluxes (cm) for 100% ET_C.

3.2. Nutrient Uptake and Calibration of Transformation Parameters

Two doses of fertilizer were applied during the growing season. The first was on 26 March, just before planting, and the complementary portion was on 16 May. While our focus is on nitrate uptake by the plant under regular and deficit irrigation, we focused on the forms of N from the applied fertilizers for inclusion in the simulation. The 350 kg ha^{-1} MAP provided 39 kg ha^{-1} of N in the form of NH_4^+ and the 103 kg ha^{-1} of UAN-32 provided 33 kg ha^{-1} N in the form of urea (16.5 kg ha^{-1}, half of the weight), ammonium (8.25 kg ha^{-1}, a quarter of the weight), and nitrate (8.25 kg ha^{-1}, a quarter of the weight). The concentrations of N were then calculated based on the volumes of irrigation water applied in kg m^{-3} (field) = mg cm^{-3} (simulation) for the whole field as well as for the entire 2D simulation domain. For nutrient applications, 0.0637 mg cm^{-3} of NH_4^+ was assigned on 26 March, 0.02727 mg cm^{-3} of $(NH_2)_2CO$, 0.01365 mg cm^{-3} of NH_4^+, and 0.01365 mg cm^{-3} of NO_3^- were assigned on 16 May. In addition, 0.0002 mg cm^{-3} NO_3^- from irrigation water was assigned with every irrigation event (11 sprinkler events, and 9 and 5 drip events for the 100% ET_C and 65% ET_C treatments, respectively).

The transformation processes of the nitrogen cycle are very complex and challenging, especially to include all the governing processes. The initial parameters for pathway reactions were assigned as constants for both soil layers [47,48,53], with one exception. The calibration process was executed for denitrification, which is the most sensitive process for the final product of nitrate in soil. Nitrate concentrations that were measured from the collected soil samples on 9 April and 28 June (Table 4) were used for model calibration of the first-order decay rate constant of denitrification ($\mu_{w,3}$ and $\mu_{s,3}$) in liquid and solid phases for the two soils in the profile. The coefficients of determination were calculated separately for the two dates and for the different locations, with north-east (N-E) and south-east (S-E) representing the 100% ET_C treatment and north-west (N-W) and south-west (S-W) representing the 65% ET_C treatment. The r^2 values of 0.9327 and 0.6861 show a good correlation between HYDRUS simulated and measured nitrate on 9 April and 28 June (Figure 6a,b) and the corresponding calibrated values of $\mu_{w,3}$ and $\mu_{s,3}$ are 0.02 and 0.02, and 0.01 and 0.01 for silty clay loam and silty clay soil, respectively.

Table 4. NO_3^- concentrations in mg L^{-1} for the collected soil sampled on 9 April and 28 June from the four locations and the corresponding HYDRUS simulated values.

Depth (cm)	Samples on 9 April (Day 15 in Simulation)							Samples on 28 June (Day 95 in Simulation)					
	(N-E)	(N-W)	Center	(S-E)	(S-W)	Avg.	HYDRUS	(N-E)	(S-E)	Avg.	HYDRUS (100% ET_C)	(N-W)	HYDRUS (65% ET_C)
0–30	59.6	73.2	36.6	36.1	48.0	**50.7**	34.5	11.4	10.6	**11.0**	9.5	**41.1**	35.6
30–60	18.2	29.5	12.5	28.5	48.2	**27.4**	25.6	22.0	25.2	**23.6**	15.5	**30.9**	15.5
60–90	15.8	10.2	5.5	29.8	47.2	**21.7**	19.9	10.6	23.6	**17.1**	15.5	**11.0**	15.5
90–105	15.4	14.6	4.8	30.8	46.8	**22.5**	18.6	9.6	28.2	**18.9**	15.5	**18.7**	15.5

* Note: concentrations from HYDRUS obtained along the vertical section 15 cm from the drip lines (plant rows) to coincide with the locations of collected soil samples. Bold values were used for calculation of correlation between measured and simulated from HYDRUS.

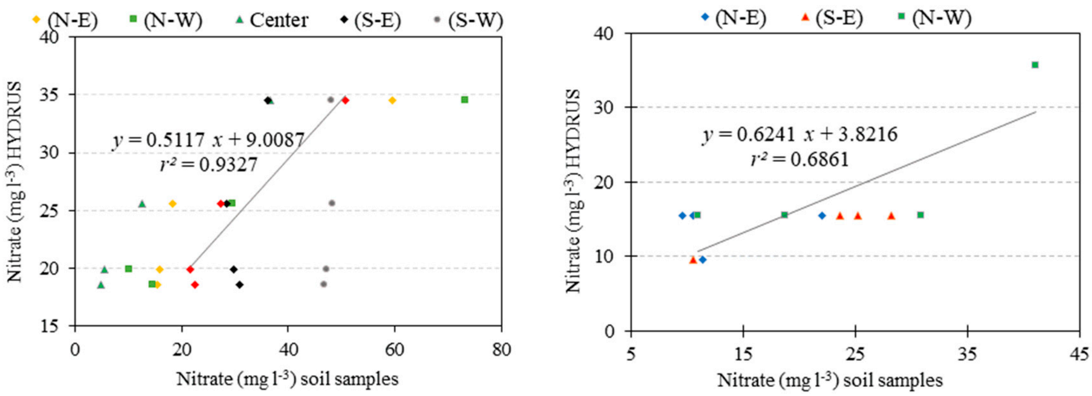

(**a**) (**b**)

Figure 6. Simulated (HYDRUS) vs. observed (soil samples) NO_3^- concentrations (**a**) for 9 April (day 15 of the simulation), and (**b**) for 28 June (day 95 of the simulation). Note that the coefficient of determination, r^2, was calculated based on the average NO_3^- for the soil samples from the different locations.

After model calibration, the concentrations of N in the three forms of $(NH_2)_2CO$, NH_4^+, and NO_3^- were recorded for each day of simulation and after the end of all irrigation events. The results of some of these simulations, at specified dates, are shown in Figure 7a–c for urea, ammonium, and nitrate, respectively. Results are shown in the ordering of pathway reaction of N, with urea shown first, followed by ammonium and then nitrate. The maximum concentration of urea, 0.021 mg cm^{-3}, was observed just after its application in the fourth drip event on 16 May, but only adjacent to the emitter (Figure 7a). The accompanying illustration of concentrations along the vertical section, 15 cm from the left side boundary and drip lines (along plant rows) is also provided in Figure 7a–c. All urea was hydrolyzed to ammonium within seven days, between 16 May and 23 May (Figure 8a), and no detectable concentrations were retained in the soil or drained downward. Like the urea, ammonium had the same behavior as the first-order decay process, nitrification to nitrate. The maximum concentration of NH_4^+ was obtained after the end of the first 24-h irrigation event on 27 March (Figure 7b) and almost all ammonium nitrified to nitrate after fourteen days (Figure 8b) when the cumulative nitrified ammonium was 9.04 mg cm^{-1} (Figure 8b). After UAN application, a small concentration of ammonium was added around the emitter (for the first soil layer) and those concentrations nitrified within twelve days (Figure 8b).

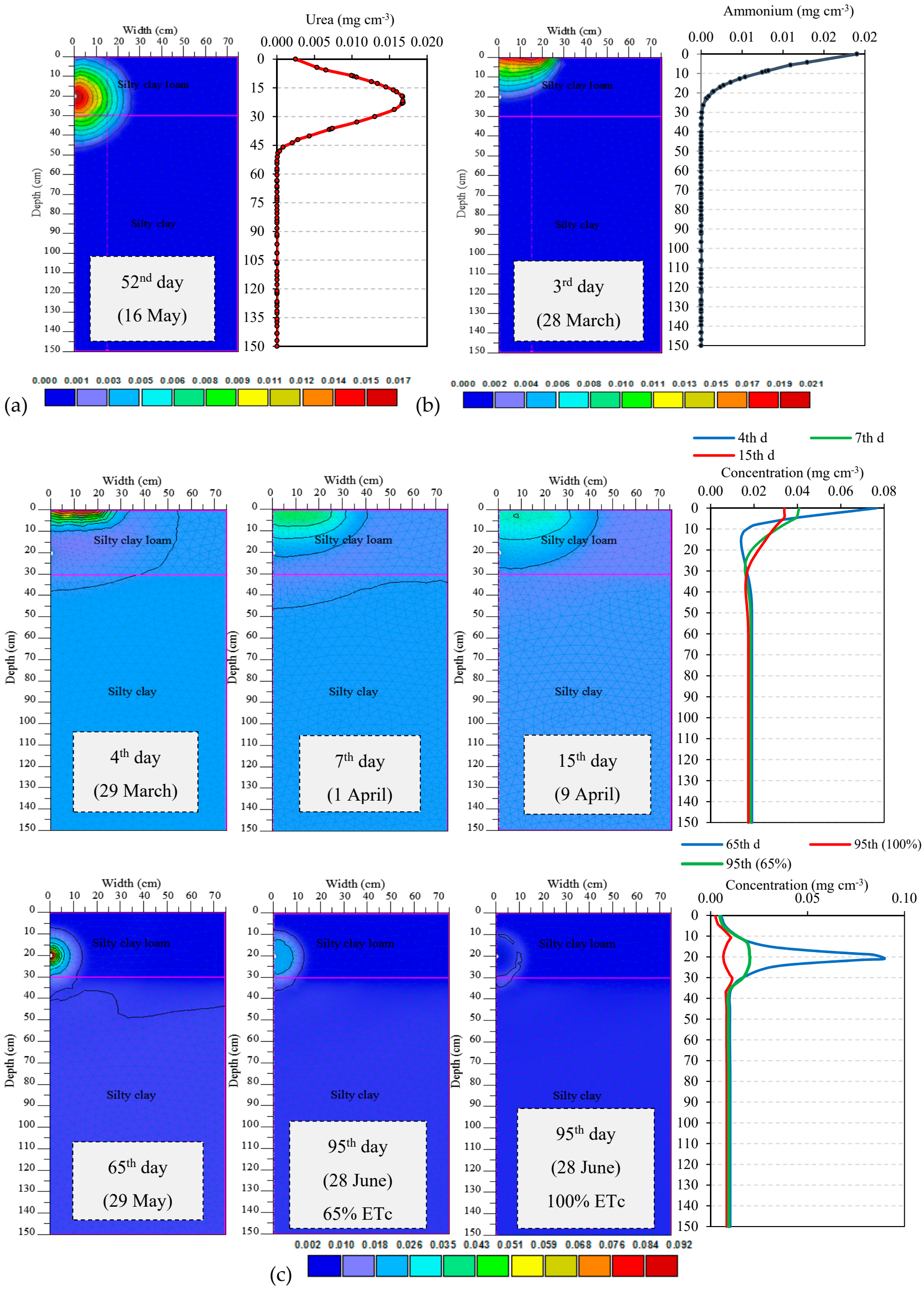

Figure 7. Representative results of the simulations of N concentrations for specified dates. (**a**) Maximum concentrations of $(NH_2)_2CO$ on 16 May. (**b**) Maximum concentrations of NH_4^+ on 28 March. (**c**) Concentrations of NO_3^- on different days throughout the simulation.

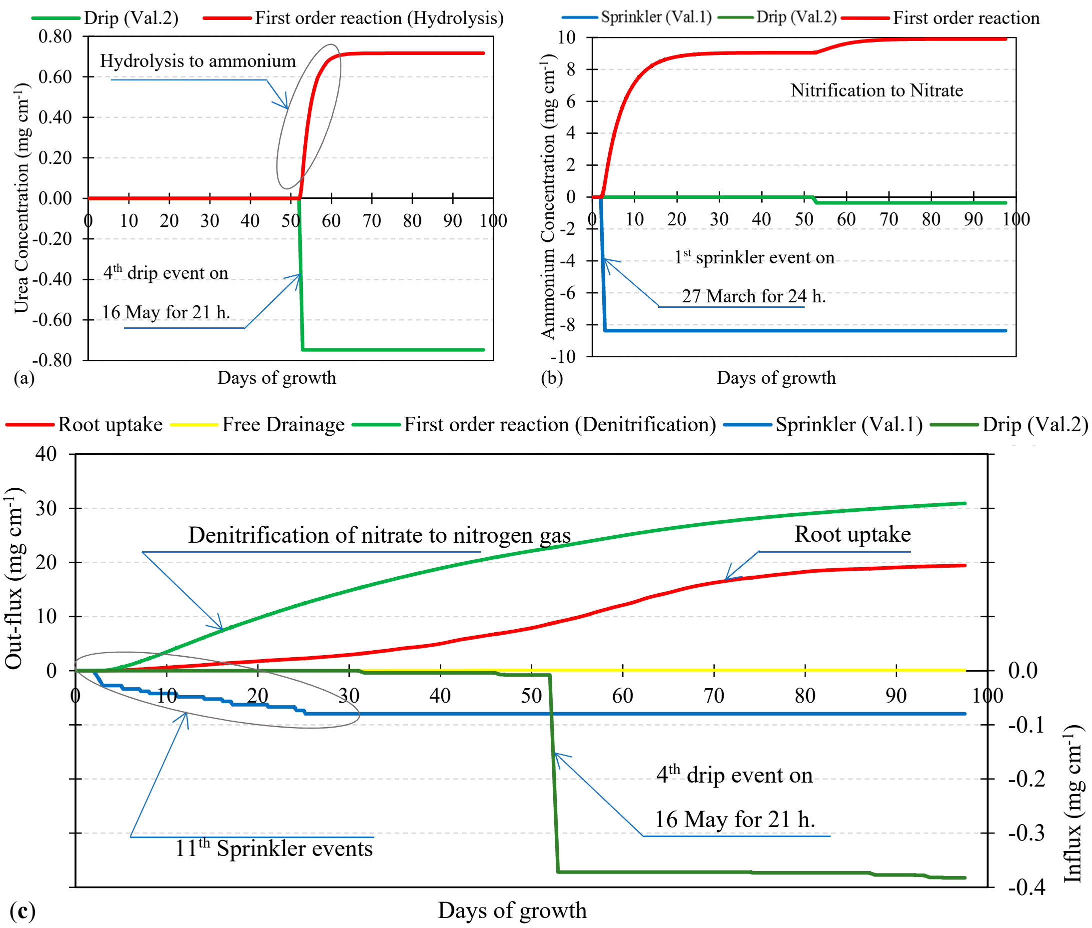

Figure 8. In- and out-fluxes of the various forms of N. (**a**) Cumulative values for $(NH_2)_2CO$ (mg cm^{-1}) (**b**) Cumulative values for NH_4^+ (mg cm^{-1}). (**c**) Cumulative values for NO_3^- (mg cm^{-1}).

As nitrate concentration is our focus here, additional results for different times during the growing season are presented in Figure 7c. The fourth day after planting (29 March) showed the maximum nitrate concentration; this occurred around the emitter from the nitrification of the applied ammonium. Although the nitrification process was still ongoing, the nitrate concentration was lower around the emitter because of the plant uptake and diffusion that drove nitrate away from the emitter which appeared on the 7th and 15th days after planting. When nitrate is present near the active root zone, root nitrate uptake occurs, and denitrification takes place. Therefore, the pattern of distribution and the remaining concentration of nitrate are highly dependent on the denitrification first-order decay parameters for both liquid and solid state (Figure 7c). The different cumulative fluxes of nitrate (mg cm^{-1}) are presented in Figure 8c, where the out-flux of nitrate by denitrification and free drainage for the case of 100% ET_C were 30.80 mg cm^{-1} and 0.085 mg cm^{-1}, respectively. The maximum obtained nitrate concentration drained out of the domain was 0.0025 mg cm^{-1} day^{-1} when the dispersivity of soil and the diffusion of nitrate in water were more dominant than denitrification. Regarding the root nitrate uptake, the cumulative fluxes were 19.44 mg cm^{-1} and 16.12 mg cm^{-1} for the 100% ET_C and 65% ET_C, respectively (Figure 8c), corresponding to a 17.1% reduction in the cumulative uptake of nitrate by the roots under deficit irrigation.

4. Discussion

Throughout the growing season, the fully irrigated portion of the field received 175 mm-ha/ha and 379 mm-ha/ha of irrigation water (100% ET_C) by sprinkler and SDI, respectively (11 sprinkler events and 9 SDI events). The assignment of the initial uniform moisture content, θ_i, and the frequent sprinkler irrigation during this early stage of growth is mainly responsible for the uniform distribution of θ along the 150 cm depth of the model domain [54]. The total available water to drain outside the bottom boundary of the domain was minimal for both the 100% ET_C and 65% ET_C treatments (2.032 cm and 2.365 cm). The drainage flux was maximized during sprinkler irrigation (from 27 March to 24 April) and the first thirty days from 25 April to 24 May that included four drip events. After this date (from 26 May to 1 July), there were no drainage fluxes because the volumetric water content did not exceed the maximum field capacity of 0.325 cm^3 cm^{-3} and 0.351 cm^3 cm^{-3} for the silty clay loam and silty clay soil, respectively; this agrees with previous results [55]. The replenishment of the moisture content via SDI was localized to the immediate vicinity of the emitters and the upper 50% of the root zone. This is attributed to the intensity of the emitter discharge, which equaled 0.42 L h^{-1}, and their close spacing. Our interpretation agrees with the results of Neshat and Nasiri [56]. The variability of soil moisture distribution patterns during sprinkler events are different than those during the SDI events, likely due to variations in irrigation system flux rates and the differences in boundary conditions where the irrigation water was applied.

For the full irrigation treatment, the simulated root water uptake flux (Figure 5b) was very similar to the potential evapotranspiration, which indicates that the plants were not under stress [57]. The simulated water uptake was likewise very similar to the actual water uptake based on soil moisture measurements for the fully irrigated treatment. However, there was a noticeable difference between the simulated root water uptake and the potential evapotranspiration for the deficit irrigation treatment (Figure 5a). The observed difference between the actual water uptake and the expected root water uptake from the simulation for the 65% ET_C irrigation treatment reflects the potential for water stress during the deficit irrigation, from 7 June through harvest. The simulated cumulative root water uptake was 36.7% lower in the deficit irrigation treatment as compared to the full irrigation treatment (53.26 cm and 33.73 cm for 100% ET_C and 65% ET_C, respectively). This reduction in water uptake in the deficit irrigation treatment is mainly attributed to the assignment of Feddes' parameters for root water uptake reduction in the model. In addition, the model did not consider possible groundwater contributions in the simulation since the bottom boundary was assigned as a free drainage condition. In addition, the root distribution parameters were uniformly assigned based on the mid-growth values with no dynamic effect because of the limitation of this feature in the model that we used (more details about the algorithm can be found in [58]). This uniform assignment of the root distribution parameters of the Vrugt model affects estimates of the root water uptake and subsequently the nutrient uptake. This may have contributed to the reduced correspondence between the simulated and observed concentrations of nitrate in the soil profile (r^2 = 0.6861). A stronger correlation between simulated and observed nitrate concentration could likely be achieved if dynamic root growth was included in the model. Additionally, different moisture distribution and root-water uptake values would be obtained when assigning different conditions for the bottom model boundary.

The average organic matter in the soil was less than 1.50% (Supplementary Table S1) and the difference between the maximum and minimum values between the top layer and the second layer was 0.2%. Therefore, the variation in organic matter is unlikely to have impacted mineralization and would not be expected to influence observed patterns of N accumulation [32]. It is also worth noting that the 16 May (fourth SDI event) application of urea was followed by a long interval until the subsequent SDI event on 7 June. As such, all of the applied urea was transformed into ammonium during this period by hydrolysis [44], a process which mainly depends on soil oxygen concentration [59]. Detectable concentrations of ammonium were only obtained close to the soil surface (during sprinkler irrigation events) after the MAP application or around the emitters after UAN-32 because of retardation due to adsorption on soil particles [60]. The subsequent nitrification occurred wherever the ammonium was present; therefore, the concentration of nitrate in the collected soil samples was higher in the topsoil than in lower layers for the 9 April measurements (first soil test).

Overall, the observed 17% reduction in cumulative nitrate root uptake under deficit irrigation could help growers by allowing them to reduce N applications, thereby improving NUE and increasing economic return when deficit irrigation is applied near the end of the growing season. Different nitrogen application strategies would likely be necessary if deficit irrigation was implemented during earlier stages of growth, or throughout the entire growing season. Previous studies conducted under maize–wheat rotation [61] showed that regulated deficit irrigation (RDI) increased N recovery by 17% compared to full irrigation. Additionally, alternating partial root-zone irrigation and full irrigation has been found to increase the ratio of N uptake to the amount of N supplied by 16% as compared to the full irrigation of maize [62,63]. Frequent drying and wetting cycles of root zones with regulated deficit irrigation improve the ability of the plant to acquire nutrients from the soil, as drying and wetting cycles of soils enhance microbial activity with microbial substrate availability, thus improving the net mineralization and increasing the N available to plants [64].

5. Conclusions and Recommendations

Nitrogen transformations were studied under full and deficit irrigation practices to investigate the effect of deficit irrigation on sunflower nitrate uptake and distribution in the first 1.50 m of soil depth under semi-arid conditions in the low desert of southern California. HYDRUS/2D simulations were used for modeling the water and nutrient root uptake including the pathway reactions among the different forms of nitrogen in the soil. The moisture content was almost uniform for the top 50 cm of soil depth during the first month of the growing season, which utilized sprinkler irrigation, while non-uniformity in soil moisture distribution was observed during the SDI period. Soil water content did not exceed field capacity, and the free drainage out the bottom boundary of the domain to recharge the groundwater corresponded to just 4.3% and 5.6% of the applied irrigation water for the 100% ET_C and 65% ET_C irrigation treatments, respectively. The maximum cumulative drainage flux was reached during the sprinkler irrigation period, while no significant drainage was observed during the SDI irrigation period. The cumulative root water uptake was 53.26 cm and 33.73 cm for 100% ET_C and 65% ET_C, respectively, which resulted in a 36.6% reduction in root water uptake due to the implementation of the deficit irrigation treatment.

Hydrolysis of urea took approximately 7 days, while the nitrification of ammonium to nitrate occurred within 14 days. The adsorption coefficient of ammonium was highly affected by the location and distribution of ammonium near the soil surface (during the sprinkler irrigation for the pre-planting MAP application) or near the emitter (during the application of UAN via SDI). Implementing deficit irrigation during the late-season stage of growth altered sunflower plant nitrogen uptake. The cumulative nitrate uptake was 19.44 mg cm^{-1} and 16.12 mg cm^{-1} for the 100% ET_C and 65% ET_C treatments, respectively; thus, there was a reduction in cumulative nitrate root uptake under deficit irrigation of approximately 17%. These results are likely specific to the timing of our deficit scenario, and we would expect different results if the deficit was applied during mid-season growth when the ET_C is highest. Regulated deficit irrigation that is applied during the early growth stages, for example, may result in more nutrient use efficiency and less nitrate leaching to groundwater. We focused our work on deficit irrigation during the late stage of growth since this is a more practical tool for growers to implement than early-stage or season-long regulated deficit irrigation. Regulated deficit irrigation during the entire season or early growth stages is not practical for growers in the low desert region of California since it requires the same number of irrigations, but at reduced application rates. The benefits associated with late-stage deficit irrigation include water, energy, and labor savings due to the reduced number of irrigation events. Given the reduced uptake of nitrogen, the application rate of nitrogen during fertigation can also be adjusted downward during the late growing stage. While late-stage deficit irrigation may be practical and economically feasible for growers in the low desert region in California, additional work is needed to study the economic benefits of various types of deficit irrigation practices on water and nitrogen use efficiency as well as the net economic benefits to growers.

Note that, while deficit irrigation scenarios in which irrigation water is reduced up to 35% (i.e., 65% ET_C) are expected to negatively impact yield, this practice could be used when water resources are limited or during drought conditions. This practice could also be implemented in more moderate climatic conditions with potentially less impact on yield since the evaporative demand would presumably be lower. Similarly, a transition to earlier planting dates could reduce potential yield losses as a result of deficit irrigation. Additional work is needed to find the optimum level of deficit irrigation practices that result in water and fertilizer savings without an overly costly reduction in yield. Indeed, both reduced irrigation water requirements and reductions in nitrogen uptake (and thus the need to fertilize) could provide a dual incentive to growers who modify their irrigation practices.

Supplementary Materials: The following are available online at http://www.mdpi.com/2073-4441/11/11/2340/s1, Table S1: Soil classification, including physical and chemical properties.

Author Contributions: Conceptualization, M.G.E., K.M.B., and J.M.B.; methodology, M.G.E., K.M.B., and J.M.B.; software, M.G.E.; validation, K.M.B., and J.M.B.; formal analysis, M.G.E.; investigation, M.G.E., K.M.B., and J.M.B.; resources, M.G.E., K.M.B., and J.M.B.; data curation, M.G.E. and K.M.B.; writing—original draft preparation, M.G.E.; writing—review and editing, K.M.B. and J.M.B.; visualization, M.G.E.; supervision, K.M.B.; project administration, K.M.B. and J.M.B.; funding acquisition, K.M.B. and J.M.B.

Funding: This work was partially supported through a grant from the U.S. National Science Foundation (Award Number 1444522).

Acknowledgments: We also would like to acknowledge support from the US Fulbright program that provided funding for the senior author to conduct this work during his stay in California. We thank the staff of the University of California Desert Research and Extension Center for providing the necessary resources for conducting this experiment.

Conflicts of Interest: The authors declare no conflict of interest.

References

1. Razaq, M.; Zhang, P.; Shen, H.L. Influence of nitrogen and phosphorus on the growth and root morphology of *Acer mono*. *PLoS ONE* **2017**, *12*, e0171321. [CrossRef] [PubMed]
2. Mullins, G. Phosphorus, Agriculture & the Environment. Virginia Cooperative Extension. 2009. Available online: https://efotg.sc.egov.usda.gov/references/public/va/PhosphorousAgEnv.pdf (accessed on 20 November 2013).
3. He, M.; Dijkstra, F.A. Drought effect on plant nitrogen and phosphorus: A meta-analysis. *New Phytol.* **2014**, *204*, 924–931. [CrossRef] [PubMed]
4. Demir, A.O.; Goksoy, A.T.; Buyukcangaz, H.; Turan, Z.M.; Köksal, E.S. Deficit irrigation of sunflower (*Helianthus annuus* L.) in a sub-humid climate. *Irrig. Sci.* **2006**, *24*, 279. [CrossRef]
5. Rouphael, Y.; Cardarelli, M.; Schwarz, D.; Franken, P.; Colla, G. Effects of drought on nutrient uptake and assimilation in vegetable crops. In *Plant Responses to Drought Stress*; Aroca, R., Ed.; Springer: Berlin/Heidelberg, Germany, 2012; pp. 171–195.
6. Sardans, J.; Penuelas, J. The role of plants in the effects of global change on nutrient availability and stoichiometry in the plant-soil system. *Plant Physiol.* **2012**, *160*, 1741–1761. [CrossRef] [PubMed]
7. Farooq, M.; Hussain, M.; Wahid, A.; Siddique, K.H.M. Drought stress in plants: An Overview. In *Plant Responses to Drought Stress*; Aroca, R., Ed.; Springer Press: Berlin/Heidelberg, Germany, 2012.
8. Schimel, J.P.; Balser, T.C.; Wallenstein, M. Microbial stress response physiology and its implications for ecosystem function. *Ecology* **2007**, *88*, 1386–1394. [CrossRef] [PubMed]
9. Lambers, H.; Chapin, F.S.; Pons, T.L. *Plant Physiological Ecology*; Springer: New York, NY, USA, 2008.
10. Farooq, M.; Aziz, T.; Wahid, A.; Lee, D.J.; Siddique, K.H.M. Chilling tolerance in maize: Agronomic and physiological approaches. *Crop Pasture Sci.* **2009**, *60*, 501–516. [CrossRef]
11. Austin, A.T.; Yahdjian, L.; Stark, J.M.; Belnap, J.; Porporato, A.; Norton, U.; Ravetta, D.A.; Schaeffer, S.M. Water pulses and biogeochemical cycles in arid and semiarid ecosystems. *Oecologia* **2004**, *141*, 221–235. [CrossRef]

12. Delgado-Baquerizo, M.; Maestre, F.T.; Gallardo, A.; Bowker, M.A.; Wallenstein, M.D.; Quero, J.L.; Ochoa, V.; Gozalo, B.; García-Gómez, M.; Soliveres, S.; et al. Decoupling of soil nutrient cycles as a function of aridity in global drylands. *Nature* **2013**, *502*, 672–676. [CrossRef]
13. Zeng, W.; Xu, C.; Huang, J.; Wu, J.; Ma, T. Emergence rate, yield, and nitrogen-use efficiency of sunflowers (*Helianthus annuus*) vary with soil salinity and amount of nitrogen applied. *Commun. Soil Sci. Plant Anal.* **2015**, *46*, 1006–1023. [CrossRef]
14. Lazicki, P.A.; Geisseler, D. Soil nitrate testing supports nitrogen management in irrigated annual crops. *Calif. Agric.* **2016**, *71*, 90–95. [CrossRef]
15. Mathers, A.C.; Stewart, B.A. Sunflower nutrient uptake, growth, and yield as affected by nitrogen or manure, and plant populations. *Agron. J.* **1982**, *74*, 911–915. [CrossRef]
16. Schneekloth, J.P. Response of Irrigated Sunflowers to Water Timing. Central Great Plains Research Station 2002 Annual Report. Colorado State University: Akron, CO, USA 4 pgs. Available online: https://www.ksre.k-state.edu/irrigate/oow/p05/Schneekloth1.pdf (accessed on 1 June 2019).
17. Zeng, W.; Xu, C.; Wu, J.; Huang, J. Sunflower seed yield estimation under the interaction of soil salinity and nitrogen application. *Field Crop. Res.* **2016**, *198*, 1–15. [CrossRef]
18. Abbadi, J.; Gerendás, J.; Sattelmacher, B. Effects of nitrogen supply on growth, yield and yield components of safflower and sunflower. *Plant Soil* **2008**, *306*, 167–180. [CrossRef]
19. Vigil, M.F.; Benjamin, J.; Schepers, J. Yield response and fertilizer nitrogen recovery by dry land sunflowers in a no-till rotation. In Proceedings of the 23rd Sunflower Production Workshop, Fargo, ND, USA, 17–18 January 2001; Vol. 23, pp. 90–94.
20. Rachael, L.; Gulya, T.; Light, S.; Bali, K.; Mathesius, K.; Meyer, R. Sunflower Hybrid Seed Production in California. 2019. Available online: https://anrcatalog.ucanr.edu/Details.aspx?itemNo=8638 (accessed on 1 June 2019).
21. Eltarabily, M.G.A.; Negm, A.M.; Valeriano, O.C.S.; Gafar, K.E. Effects of di-ammonium phosphate on hydraulic, compaction, and shear strength characteristic of sand and clay soils. *Arab. J. Geosci.* **2015**, *8*, 10419–10432. [CrossRef]
22. Blamey, F.P.C.; Chapman, J. Protein, Oil, and Energy Yields of Sunflower as Affected by N and P Fertilization1. *Agron. J.* **1981**, *73*, 583. [CrossRef]
23. Davidson, E.A.; Seitzinger, S. The enigma of progress in denitrification research. *Ecol. Appl.* **2006**, *16*, 2057–2063. [CrossRef]
24. Gentry, L.E.; David, M.B.; Below, F.E.; Royer, T.V.; McIsaac, G.F. Nitrogen Mass Balance of a Tile-drained Agricultural Watershed in East-Central Illinois. *J. Environ. Qual.* **2009**, *38*, 1841–1847. [CrossRef]
25. Jaynes, D.; Colvin, T.; Karlen, D.; Cambardella, C.; Meek, D. Nitrate loss in subsurface drainage as affected by nitrogen fertilizer rate. *J. Environ. Qual.* **2001**, *30*, 1305–1314. [CrossRef]
26. Webb, J.; Ellis, S.; Harrison, R.; Thorman, R. Measurement of N fluxes and soil N in two arable soils in the UK. *Plant Soil* **2004**, *260*, 253–282. [CrossRef]
27. Hama, T.; Nakamura, K.; Kawashima, S.; Kaneki, R.; Mitsuno, T. Effects of cyclic irrigation on water and nitrogen mass balances in a paddy field. *Ecol. Eng.* **2011**, *37*, 1563–1566. [CrossRef]
28. Letey, J.; Vaughan, P. Soil type, crop and irrigation technique affect nitrogen leaching to groundwater. *Calif. Agric.* **2013**, *67*, 231–241. [CrossRef]
29. Prasad, R.; Hochmuth, G.J.; Boote, K.J. Estimation of Nitrogen Pools in Irrigated Potato Production on Sandy Soil Using the Model SUBSTOR. *PLoS ONE* **2015**, *10*, e0117891. [CrossRef] [PubMed]
30. Negm, A.M.; Yoshimura, C.; Saavedra, O.C.; Eltarabily, M.G. Modeling the impact of nitrate fertilizers on groundwater quality in the southern part of the Nile Delta, Egypt. *Water Supply* **2016**, *17*, 561–570.
31. Follet, R.F. Transformation and transport processes of nitrogen in agricultural systems. In *Nitrogen in the Environment: Sources, Problems, and Management*; Hatfield, J.L., Follet, R.F., Eds.; Academic Press: San Diego, CA, USA, 2008. Available online: http://digitalcommons.unl.edu/usdaarsfacpub/261 (accessed on 1 June 2019).
32. Robertson, G.P.; Groffman, P.M. Nitrogen transformation. In *Soil Microbiology, Biochemistry, and Ecology*; Paul, E.A., Ed.; Springer: New York, NY, USA, 2007; pp. 341–364.

33. Simunek, J.; Sejna, M.; Saito, H.; Sakai, M.; van Genuchten, M.T. *The HYDRUS-1D Software Package for Simulating the Movement of Water, Heat, and Multiple Solutes in Variably Saturated Media*; Version 4.0; HYDRUS Software Series 3; Department of Environmental Sciences, University of California Riverside: Riverside, CA, USA, 2008.
34. Baram, S.; Couvreur, V.; Harter, T.; Read, M.; Brown, P.; Kandelous, M.; Smart, D.; Hopmans, J. Estimating Nitrate Leaching to Groundwater from Orchards: Comparing Crop Nitrogen Excess, Deep Vadose Zone Data-Driven Estimates, and HYDRUS Modeling. *Vadose Zone J.* **2016**, *15*, 11. [CrossRef]
35. Jha, R.K.; Sahoo, B.; Panda, R.K. Modeling the water and nitrogen transports in a soil–paddy–atmosphere system using HYDRUS-1D and lysimeter experiment. *Paddy Water Environ.* **2017**, *15*, 831–846. [CrossRef]
36. Šimůnek, J.; Van Genuchten, M.T.; Šejna, M. Recent Developments and Applications of the HYDRUS Computer Software Packages. *Vadose Zone J.* **2016**, *15*, 15. [CrossRef]
37. Eltarabily, M.G.; Bali, K.M.; Negm, A.M.; Yoshimura, C. Evaluation of Root Water Uptake and Urea Fertigation Distribution under Subsurface Drip Irrigation. *Water* **2019**, *11*, 1487. [CrossRef]
38. Ullah, H.; Santiago-Arenas, R.; Ferdous, Z.; Attia, A.; Datta, A. Chapter Two—Improving water use efficiency, nitrogen use efficiency, and radiation use efficiency in field crops under drought stress: A review. *Adv. Agron.* **2019**, *156*, 109–157.
39. Galloway, J.N.; Townsend, A.R.; Erisman, J.W.; Bekunda, M.; Cai, Z.; Freney, J.R.; Martinelli, L.A.; Seitzinger, S.P.; Sutton, M.A. Transformation of the Nitrogen Cycle: Recent Trends, Questions, and Potential Solutions. *Science* **2008**, *320*, 889–892. [CrossRef]
40. Gastal, F.; Lemaire, G. N uptake and distribution in crops: An agronomical and ecophysiological perspective. *J. Exp. Bot.* **2002**, *53*, 789–799. [CrossRef]
41. Huang, T.; Ju, X.; Yang, H. Nitrate leaching in a winter wheat-summer maize rotation on a calcareous soil as affected by nitrogen and straw management. *Sci. Rep.* **2017**, *7*, 42247. [CrossRef] [PubMed]
42. Available online: https://websoilsurvey.nrcs.usda.gov/app/WebSoilSurvey.aspx (accessed on 1 June 2019).
43. Available online: https://cimis.water.ca.gov/Stations.aspx (accessed on 1 July 2019).
44. Snyder, L.; Orang, M.; Bali, K.; Basic Irrigation Scheduling Program (BISe). Oakland: University of California Land, Air, and Water Resources Biomet Website. 2014. Available online: http://biomet.ucdavis.edu/irrigation_scheduling/bis/BIS.htm (accessed on 1 June 2019).
45. Available online: https://www.iid.com/water/library/qsa-water-transfer (accessed on 1 July 2019).
46. Miller, J. Hybrid selection and production practices. In *Sunflower Production*; Berglund, D.R., Ed.; North Dakota State University (NDSU): Fargo, ND, USA, 2007; p. 117, Extension Publication A-1331. Available online: https://www.ag.ndsu.edu/pubs/plantsci/rowcrops/a1331-04.pdf (accessed on 15 July 2019).
47. Antonopoulos, V.Z. Modelling of water and nitrogen balances in the ponded water and soil profile of rice fields in Northern Greece. *Agric. Water Manag.* **2010**, *98*, 321–330. [CrossRef]
48. Hanson, B.R.; Simunek, J.; Hopmans, J.W. Evaluation of urea–ammonium–nitrate fertigation with drip irrigation using numerical modeling. *Agric. Water Manag.* **2006**, *86*, 102–113. [CrossRef]
49. Jansson, P.-E.; Karlberg, L. *Coupled Heat and Mass Transfer Model for Soil-Plant-Atmosphere Systems*; Department of Civil and Environmental Engineering, KTH Royal Institute of Technology: Stockholm, Sweden, 2001; p. 321.
50. Zeng, W.; Lei, G.; Zha, Y.; Fang, Y.; Wu, J.; Huang, J. Sensitivity and uncertainty analysis of the HYDRUS-1D model for root water uptake in saline soils. *Crop. Pasture Sci.* **2018**, *69*, 163. [CrossRef]
51. Ventura, F.; Snyder, R.L.; Bali, K.M. Estimating Evaporation from Bare Soil Using Soil Moisture Data. *J. Irrig. Drain. Eng.* **2006**, *132*, 153–158. [CrossRef]
52. Vanaja, M.; Yadav, S.; Archana, G.; Lakshmi, N.J.; Reddy, P.R.; Vagheera, P.; Razak, S.A.; Maheswari, M.; Venkateswarlu, B. Response of C4 (maize) and C3 (sunflower) crop plants to drought stress and enhanced carbon dioxide concentration. *Plant Soil Environ.* **2011**, *57*, 207–215. [CrossRef]
53. Tan, X.; Shao, D.; Gu, W.; Liu, H. Field analysis of water and nitrogen fate in lowland paddy fields under different water managements using HYDRUS-1D. *Agric. Water Manag.* **2015**, *150*, 67–80. [CrossRef]
54. Carr, M.K.V. Crop yield response to water. In *FAO Irrigation and Drainage Paper 66*; Steduto, P., Hsiao, T.C., Fereres, E., Raes, D., Eds.; Food and Agriculture Organization of the United Nations: Rome, Italy, 2012; p. 500. Available online: http://www.fao.org/docrep/016/i2800e/i2800e00.htm (accessed on 20 July 2019).

55. Oosterbaan, R.J. Agricultural drainage criteria. In *Drainage Principles and Applications*; Ritzema, H.P., Ed.; International Institute for Land Reclamation and Improvement (ILRI): Wageningen, The Netherlands, 1994; ISBN 9070754339.
56. Neshat, A.; Nasiri, S. Finding the optimal distance of emitters in the drip irrigation in loam-sandy soil in the Ghaeme Abad plain of Kerman. Iran. *Middle-East J. Sci. Res.* **2012**, *11*, 426–434.
57. Wu, J.; Zhang, R.; Gui, S. Modeling soil water movement with water uptake by roots. *Plant Soil* **1999**, *215*, 7–17. [CrossRef]
58. Simunek, J.; Hopmans, J.W. Modeling compensated root water and nutrient uptake. *Ecol. Model.* **2009**, *220*, 505–521. [CrossRef]
59. Wagenet, R.J.; Biggar, J.W.; Nielsen, D.R. Tracing the Transformations of Urea Fertilizer during Leaching1. *Soil Sci. Soc. Am. J.* **1977**, *41*, 896. [CrossRef]
60. Selim, H.M.; Iskandar, I.K. Modeling nitrogen transport and transformations in soils: 2. Validation. *Soil Sci.* **1981**, *131*, 303–312. [CrossRef]
61. Kirda, C.; Topcu, S.; Kaman, H.; Ulger, A.; Yazici, A.; Cetin, M.; Derici, M. Grain yield response and N-fertiliser recovery of maize under deficit irrigation. *Field Crop. Res.* **2005**, *93*, 132–141. [CrossRef]
62. Wang, Y.; Liu, F.; Jensen, L.S.; de Neergaard, A.; Jensen, C.R. Alternate partial root-zone irrigation improves fertilizer-N use efficiency in tomatoes. *Irrig. Sci.* **2013**, *31*, 589–598. [CrossRef]
63. Li, F.; Liang, J.; Kang, S.; Zhang, J. Benefits of alternate partial root-zone irrigation on growth, water and nitrogen use efficiencies modified by fertilization and soil water status in maize. *Plant Soil* **2007**, *295*, 279–291. [CrossRef]
64. Chai, Q.; Gan, Y.; Zhao, C.; Xu, H.; Waskom, R.M.; Niu, Y.; Siddique, K.H.M. Regulated deficit irrigation for crop production under drought stress. A review. *Agron. Sustain. Dev.* **2016**, *36*, 3. [CrossRef]